Research Article

Xue Dong, Haiyan Wang, Cheng Liu*, Hua Tao and Jianqiang Zhu

Measurement of large optical elements used for inertial confinement fusion with ptychography

https://doi.org/10.1515/aot-2017-0062
Received September 15, 2017; accepted October 17, 2017; previously published online December 4, 2017

Abstract: High-power laser drivers are located in huge laser facilities built for inertial confinement fusion, and have achieved important progresses in the past decade; however, many unconventional optical elements implemented still cannot be accurately measured. To solve this problem, the ptychographic iterative engine (PIE), which is a recently developed technique that can detect both the phase and modulus of the light field simultaneously, is adopted to measure the transmission function of these optical elements and then to accurately characterize their key parameters. The distinctive advantage of PIE over other traditional metrology techniques in measuring large optical elements is demonstrated in this paper by detecting the focal length of a lens array and the surface profile of a continuous phase plate.

Keywords: diffractive optics; phase measurement; phase retrieval; ptychographic iterative engine.

1 Introduction

High-power laser facilities built for inertial confinement fusion (ICF) use hundreds of high-power laser beams to compress the target pill filled with nuclear material symmetrically to achieve extremely high temperature and pressure to lighten nuclear fusion [1, 2]. As the peak power of these laser beams can reach 10^{16} W or higher, to avoid laser-induced damage, all laser beams should be expanded to 400 mm in diameter to reduce the energy intensity in the processes of amplification, propagation, filtering, and frequency conversion. Laser pulses from the seed laser source always pass through a huge number of optical components when reaching the target, and the whole optical path is >100 m [3]. The wavefront of laser beams can be easily distorted by various factors such as material non-uniformity and the inaccurate surface profile of optics used. Although the wavefront distortion induced by a single individual optical element is tiny, the final wavefront of laser beams reaching the target can be seriously twisted after passing numerous optical elements, and in some cases the focal spot formed on the target can be remarkably dispersed, leading to the failure of physical experiments [4, 5]. To obtain focal spots with a high enough energy concentration ratio, the wavefront of laser beams should be very accurate during the whole optical path from the seed laser source to the target [6, 7]. Accordingly, the requirement on the quality of optical elements is extremely high, and the transmission function of each optical element should be accurately measured in advance. Most optical elements used in high-power laser facilities can be accurately measured with an interferometer [8], which is a well-developed and widely applied instrument with high resolution and high reliability. The typical accuracy of a phase-shift interferometer is always $>0.05\lambda$, and the highest transverse resolution reachable is about 1 μm. However, in the field of high-power lasers, the diameter of optical elements can be 400 mm and their surface profile can be completely irregular; thus, it is very difficult to measure these unconventional optical elements with traditional interferometers. Take the random phase plate (RPP) as an example; as a key optical element to make focal spots smooth, the peak-valley value of the surface profile of RPP is about 30 wavelengths of the He-Ne laser, and the largest phase ramp of the transmission field under the planar illumination can be 10 rad/cm, which exceeds the resolvable capability of common

***Corresponding author: Cheng Liu,** Shanghai Institute of Optics and Fine Mechanics, Chinese Academy of Sciences, Shanghai 201800, China, e-mail: chengliu@siom.ac.cn
Xue Dong: Shanghai Institute of Optics and Fine Mechanics, Chinese Academy of Sciences, Shanghai 201800, China; and University of Chinese Academy of Sciences, Beijing 100049, China
Haiyan Wang and Jianqiang Zhu: Shanghai Institute of Optics and Fine Mechanics, Chinese Academy of Sciences, Shanghai 201800, China
Hua Tao: Shanghai Institute of Optics and Fine Mechanics, Chinese Academy of Sciences, Shanghai 201800, China; and State Key Laboratory of Pulsed Power Laser Technology, Electronic Engineering Institute, Anhui 230037, China

interferometers. Though, in theory, the measurement of its transmission function can be realized by dividing whole aperture into sub-apertures and stitching all measurements of every sub-aperture together, the measurement will be too complex and time consuming.

The ptychographic iterative engine (PIE) [9, 10] is a recently developed coherent diffractive imaging (CDI) technique that scans a sample through a localized illumination beam to many positions and records all diffraction patterns formed. When there is proper overlapping between two neighboring illumination regions, the complex amplitudes of both the illumination probe and that of the scanning object can be reconstructed faithfully with two counterpart updating formulas from the recorded diffraction array. Compared to traditional CDI techniques based on Fienup's hybrid input-output and error reduction algorithms [11–13], PIE has the advantages of an infinite field of view in theory, high convergence speed, and high reliability. Different iterative algorithms have also been proposed for ptychographic reconstruction, such as the difference map, which has been effectively demonstrated by experiments [14]. Like other CDI techniques, PIE is also mainly used for imaging with X-ray and high-energy electron beams [15–18]; however, it also finds many applications in the regime of visible light. In this article, we will illustrate how to use PIE to resolve some difficulties in measuring the unconventional optics used in high-power laser facilities [19].

2 Principle of extended PIE

As a modified PIE, extended PIE (ePIE) [20] was proposed to relax the high requirements for modeling the illumination. As ePIE can reconstruct illumination and object functions simultaneously with high convergence speed and high robustness to noise, it has various applications in different fields.

The geometry of PIE is shown in Figure 1. The object mounted on a translation stage has a transmission function of $O(r)$ and is illuminated by a probe $P(r)$, where r is the coordinate of the object plane. The object can be scanned laterally to many positions, and the diffraction patterns are recorded by a charge-coupled device (CCD) camera in far field. As an iterative method, PIE reconstructs the light field by propagating it forward and backward between the object plane and the detector plane.

The exit wave from the object can be written as the multiplication of $P(r)$ and $O(r)$ under "thin-object" approximation:

$$\varphi_n(r) = P_n(r) O_n(r-R), \tag{1}$$

where n indicates the nth iteration and R is the shift of probe to object.

Reconstruction can be carried out iteratively with the following steps:

(I) Propagate the exit wave $\varphi_n(r)$ to the recording plane using the Fresnel formula [21] (Fourier transform can be applied when the detector is in the far field of the object) and replace the modulus of the calculated complex field with the square root of the recorded diffraction pattern $I(u)$.

$$\Psi_n(u) = \sqrt{I(u)} \frac{FFT(\varphi_n(r))}{\left|FFT(\varphi_n(r))\right|}, \tag{2}$$

where $I(u)$ is the intensity of diffraction pattern recorded by CCD and FFT represents Fourier transform.

(II) Backpropagate $\Psi_n(u)$ to the object plane via an inverse Fourier transform:

$$\varphi_n'(r) = FFT^{-1}(\Psi_n(u)), \tag{3}$$

where FFT^{-1} represents the inverse Fourier transform.

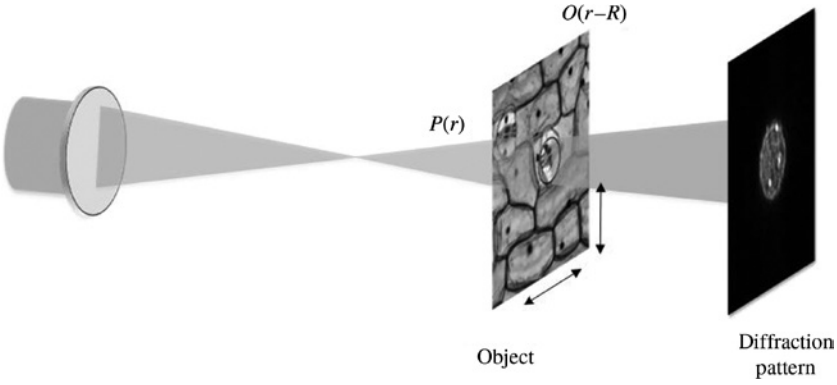

Figure 1: Schematic of standard PIE.

(III) Update $P_n(r)$ and $O_n(r-R)$ with the following two updating formulas:

$$O_{n+1}(r-R)=O_n(r-R)+\alpha\frac{P_n^*(r)}{\left|P_n(r)\right|^2_{\max}}(\varphi'_n(r)-\varphi_n(r)), \quad (4)$$

$$P_{n+1}(r)=P_n(r)+\beta\frac{O_n^*(r-R)}{\left|O_n^*(r-R)\right|^2_{\max}}(\varphi'_n(r)-\varphi_n(r)). \quad (5)$$

These two updating formulas are the origins of all fundamental advantages of PIE over other conventional CDI techniques. They use spatially varying weight functions to relax the hard-edge limitation in conventional algorithms. The constants α and β can be adjusted to alter the step size of the updating.

(IV) Repeat the above computation steps for all positions in the nth iteration.

(V) Calculate the difference of two successive $O_{n+1}(r)$ and $O_n(r)$:

$$E=\frac{\sum_r\left|O_{n+1}(r)-O_n(r)\right|^2}{\sum_r\left|O_n(r)\right|^2}. \quad (6)$$

If this difference is smaller than the given value ε, the iterative reconstruction stops; else, jump to step (I) to start another round of calculation.

3 Measurement of optical elements

As mentioned above, it is rather a challenge to accurately measure the transmission function of large optical elements used in high-power laser facilities with conventional methods. In this section, we will demonstrate how to use ePIE to realize these measurements by measuring the focal lengths of lens array and the transmission function of continuous RPP.

3.1 Basic principle of measuring optical elements with ePIE

The experimental setup to measure the transmission function of large optical elements is illustrated in Figure 2. A parallel beam is incident on a focusing lens and then transmits the optical element to be measured before reaching a diffusing object mounted on a translation stage. All diffraction patterns are recorded by a CCD during the lateral scanning of the diffusing object. Before the optical element to be measured is put into the optical path, the illumination $P_0(x_1, y_1)$ on the scanning object and the transmission function $O_0(x_1, y_1)$ of the object can be reconstructed simultaneously with the ePIE algorithm. Then, by propagating $P_0(x_1, y_1)$ to the plane exactly behind the focal lens in Figure 2, we obtain the field $U_0(x_2, y_2)$, which will illuminate on the optical element to be measured. By placing the optical element to be measured closely behind the focal lens and repeating the above measurement, the light field $U_1(x_2, y_2)$ leaving the optical element to be measured is obtained. The complex transmission function $T(x_2, y_2)$ of the optical element to be measured can be obtained by calculating $U_1(x_2, y_2)/U_0(x_2, y_2)$.

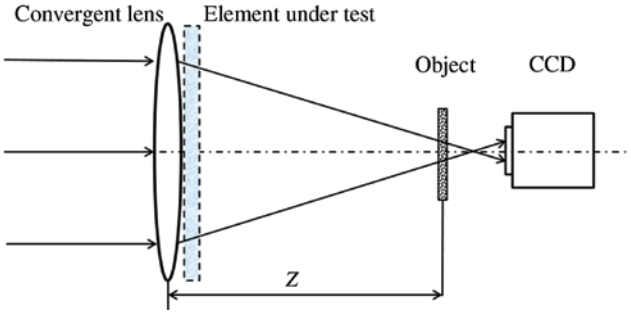

Figure 2: Fundamental configuration for measuring large optical elements.

3.2 Measurement of the focal length of the lens array

ICF needs very strict experimental conditions, and uniform irradiation on target is absolutely required. Focal spots can be efficiently smoothed [22] when the lens array in Figure 3 is placed before the main lens. As each sublens only changes the position of the original focal spot

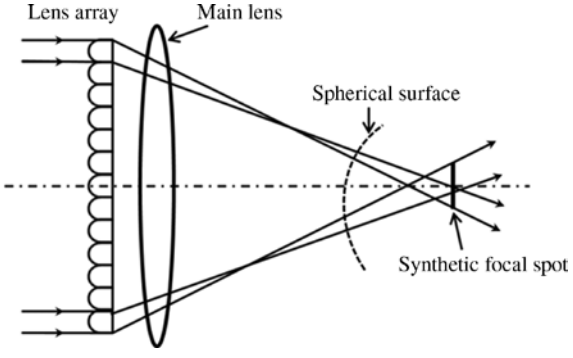

Figure 3: Lens array used in the focal system.

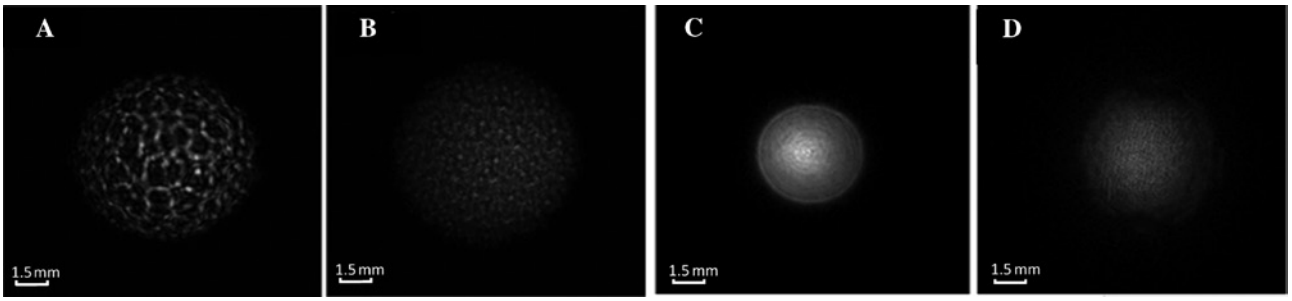

Figure 4: Diffraction patterns recorded (A) without and (B) with lens array in the optical path; illuminations incident on the scanning diffuser (C) without and (D) with lens array in the optical path.

a little, its focal length should be very long, varying from 10 m to dozens of meters. The focal lengths of lens array are not easy to measure with conventional techniques.

After the transmission function $T(x_2, y_2)$ of the lens array is measured accurately with the experimental setup in Figure 2, the focal lengths of all sub-lenses can be easily determined simultaneously by numerically propagating its transmitted field under ideally planar illumination and finding the positions of intensity peaks. In the experiment, the He-Ne laser beam is expanded and collimated to 280 mm in diameter, the focal length of the main lens in Figure 3 is 1575 mm, the scanning object mounted on translation stage is a holographic diffuser, an 8-bit CCD camera with pixels of 7.4 μm × 7.4 μm was placed downstream of the scanning object to record diffraction patterns, and the distance of the scanning object to the central focal spot of the system and CCD are 15 and 101.7 mm, respectively. One hundred diffraction patterns over a 10 × 10 position grid were recorded. Figure 4A shows one of the diffraction patterns recorded before the optical element to be measured is put in the optical path, and Figure 4B shows the diffraction patterns recorded with the optical element to be measured. The scanning objet adopted is a diffuser made using computer-generated holography. The advantage of this kind of diffuser is that its diffuse angle is designable.

Two illuminations, $P_0(x_1, y_1)$ and $P_1(x_1, y_1)$, that are incident on the scanning object can be measured with two sets of diffraction patterns recorded without and with the lens array in optical path. The moduli of the reconstructed $P_0(x_1, y_1)$ and $P_1(x_1, y_1)$ are shown in Figure 4C and D, respectively. By propagating $P_0(x_1, y_1)$ to the back plane of the main focal lens, the illumination field $U_0(x_2, y_2)$ on the lens array is obtained, and the exit field $U_1(x_2, y_2)$ of the lens array can also be obtained by propagating $P_1(x_1, y_1)$ to the back plane of the lens array. As the lens array is a pure phase object, its transmission function $T(x_2, y_2)$ can be determined by calculating the phase of the angle $\{U_0^*(x_2, y_2) \cdot U_1(x_2, y_2)\}$. The spatial resolution of the measurement can be calculated based on the Fresnel propagator, $\Delta x = \frac{\lambda z}{N \cdot \Delta x_{\text{diffuser}}} = \frac{\lambda z}{N \cdot \Delta x_{\text{ccd}}}$, where λ is the wavelength of the He-Ne laser employed, z is the distance between the main focal lens and the diffuser, N is the number of pixels in one dimension of the computing matrix, $\Delta x_{\text{diffuser}}$ is the sampling interval at diffuser plane, and Δx_{ccd} is the pixel pitch of CCD. The sampling interval at the diffuser plane and that at the CCD plane are equal when the angular propagation algorithm is applied for PIE computation. For our experiment, the spatial resolution is about 65 μm, with the following parameters: $\lambda = 632.8$ nm, $z = 1560$ mm, $N = 2048$, and $\Delta x_{\text{ccd}} = 7.4$ μm.

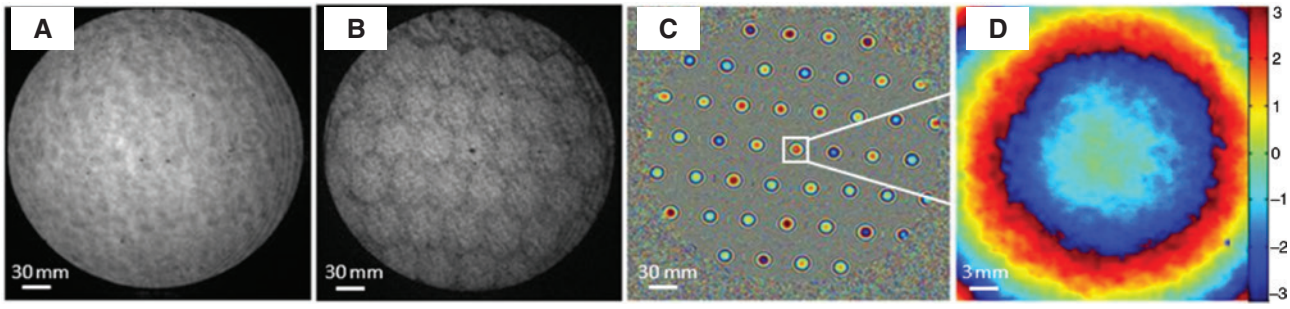

Figure 5: (A) Amplitude of the illumination field $U_0(x_2, y_2)$ and (B) exit field of the lens array $U_1(x_2, y_2)$. (C) Transmission function of the lens array and (D) phase distribution of the central sub-lens.

Figure 5A and B show the modulus of $U_0(x_2, y_2)$ and the exit field $U_1(x_2, y_2)$, respectively, and Figure 5C shows the transmission function of the lens array. Figure 5D is the zoomed-in image of the phase distribution of the central sub-lens, where we can see the details of the phase profile.

We propagate the exit field $U(x, y)$ under ideally planar illumination to the far field of 39 m away, which is the designed value of focal length. By propagating each focal spot backwards or forwards a little to search for the highest-intensity peak along the axis, the exact focal length of each sub-lens can be determined accurately. Figure 6A is the photograph of the lens array measured. Figure 6B–F show the intensity distribution of the central focal spot changing with the axis, and from them we can find that the exact focal length is 39.20 m and the diameter of focal spots is about 300 μm. The focal lengths of other sub-lenses can also be determined in the same way.

3.3 Measurement of the continuous phase plate

The continuous phase plate (CPP) is a diffractive optical element that is designed to smooth laser beams to obtain an ideal focal spot in a high-power laser system [23, 24]. In order to meet the requirements of physical experiments, CPP has a highly irregular surface profile. As its typical spatial period is about several millimeters and its phase gradient is rather huge, conventional measurement techniques are not suitable for its transmission function measurement. For example, the largest phase gradient of a CPP is about 8λ/cm; however, commonly used large-aperture interferometers can only measure the gradient of 2λ/cm. Figure 7A shows the photograph of CPP used in practical experiments, which has a diameter of 31 cm. Its designed surface profile is shown in Figure 7B, where the peak and the valley values corresponding to the He-Ne laser are 13.8714 and –15.4880 rad, respectively. Figure 7C shows the measurement of a Zygo interferometer, and black regions represent places where the surface profile is too steep to resolve. Figure 7C shows the unwrapped phase using the least square method, and as phase unwrapping is essentially a global optimization technique, the existence of an invalid measurement makes the values of the other areas incorrect; thus, there is no similarity between the designed value and the measured value.

The measurement of the transmission function of a CPP is similar to the measurement of the lens array, and all experimental parameters are the same. Figure 8A and B show two diffraction patterns recorded before and after the CPP was put into the optical path. Illuminations on the diffusive object can be reconstructed accurately

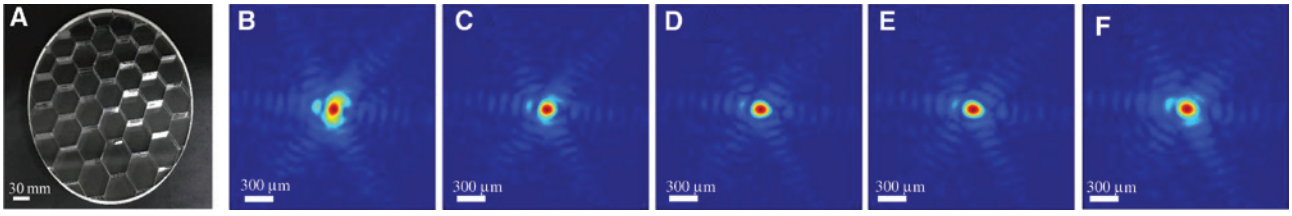

Figure 6: The lens array used and focus distribution at various distances. (A) The lens array used in the experiment. (B–F) Focus distribution at the distance of (B) 39 m, (C) 39.1 m, (D) 39.2 m, (E) 39.3 m, and (F) 39.4 m behind the convergent lens according to the phase function of the central sub-lens.

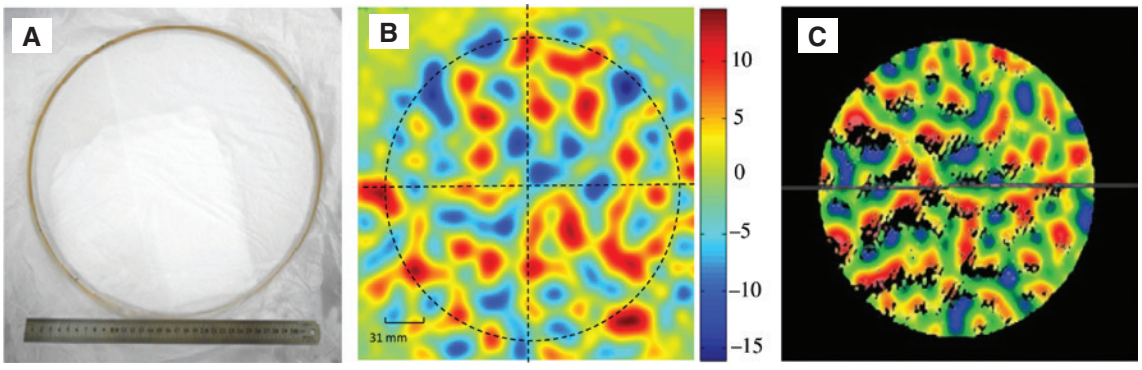

Figure 7: (A) The CPP used in the experiment; (B) the designed surface profile of CPP and (C) measurement results of CPP by the Zygo interferometer.

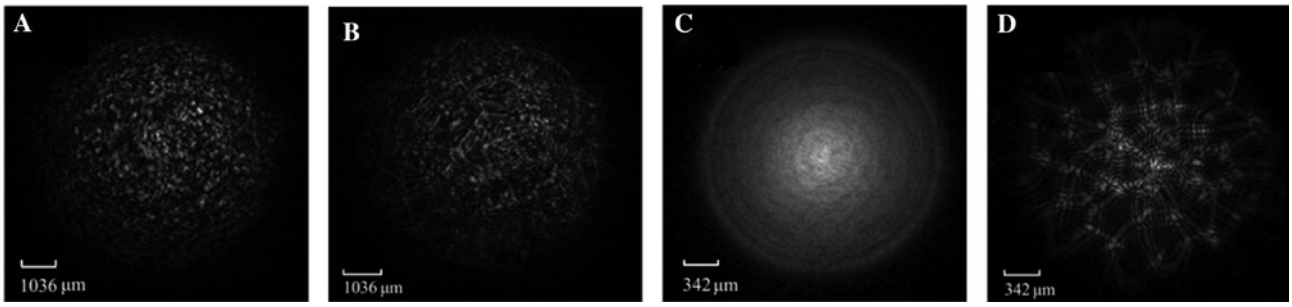

Figure 8: Diffraction patterns recorded (A) without and (B) with CPP in the optical path; amplitude of the reconstructed illuminations on the diffuser plane (C) without and (D) with CPP in the optical path.

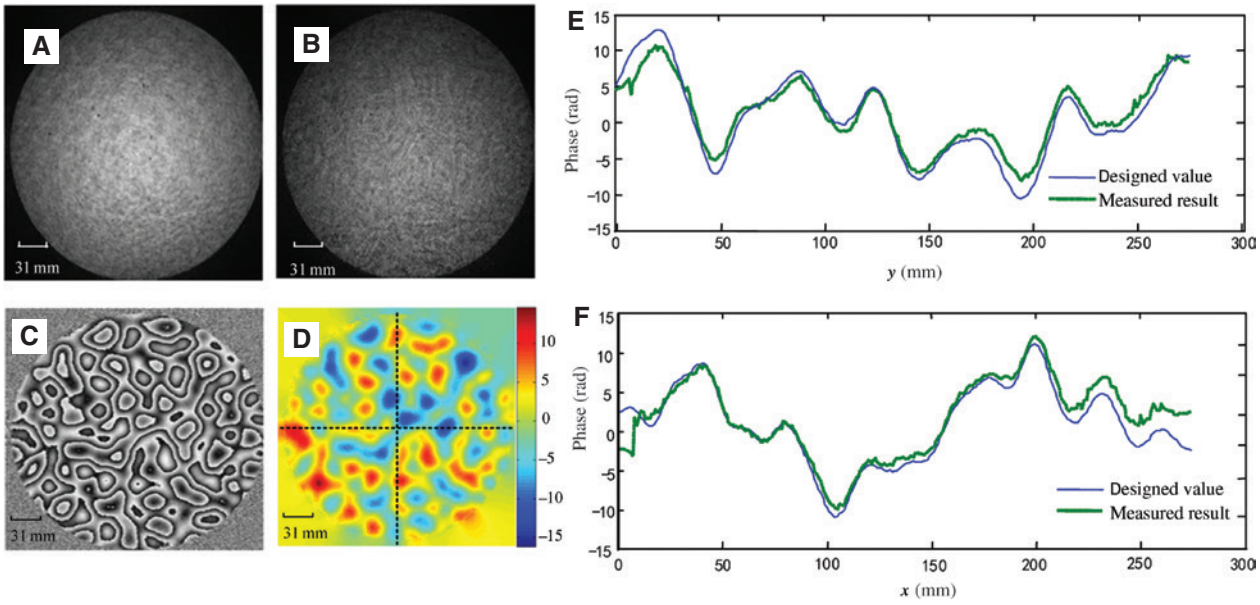

Figure 9: (A) Amplitude of the illumination field $U_0(x_2, y_2)$ and (B) exit field of $U_1(x_2, y_2)$ of CPP; (C) wrapped and (D) unwrapped phase of CPP measured by ePIE; (E) the measured result and designed value along the vertical line of Figures 7B and 9D; (F) the measured result and designed value along the horizontal line of Figures 7B and 9D.

with two sets of diffraction patterns. Figure 8C shows the modulus of the reconstructed illuminations without CPP, and Figure 8D shows the modulus of the reconstructed illuminations with CPP.

Similar to the measurement of lens array, the illumination $U_0(x_2, y_2)$ on the CPP and its exit field $U_1(x_2, y_2)$ can be obtained by propagating these two illumination beams to the back planes of the main lens and CPP, respectively. The transmission function $T(x_2, y_2)$ of CPP can be obtained by calculating the phase of angle $\{U_0^*(x_2, y_2)\cdot U_1(x_2, y_2)\}$, as CPP is a pure phase object. Figure 9C shows the wrapped phase of the measured phase distribution, and Figure 9D shows the unwrapped phase distribution. It is obvious that the measured value has high similarity to the designed value in Figure 7B. For clarity, we plot the designed value and the measured value along the horizontal and vertical lines in Figure 9E and F, respectively. We can find that the maximum difference between the measured and designed values is only about 2.1 rad, which means that the manufacturing accuracy is about one-third of the wavelength.

4 Conclusion

The ePIE algorithm was applied to measure large optical elements used in high-power laser facilities, and the advantages of this measurement technique were demonstrated by measuring the focal lengths of a lens array and the surface profile of a CPP. In these two applications, the illumination beam on the optical elements to be measured and the exit beam were obtained by applying the

ePIE algorithm twice, then the transmission function was measured by calculating their phase difference, and other key parameters of the optical elements are available. The experimental results clearly showed that PIE has remarkable advantages over conventional methods for measuring large optical elements and can find many applications in the field of high-power laser. Different kinds of iterative algorithms will be used to realize the same measurement in the future.

Acknowledgments: This work was supported by the National Natural Science Foundation of China (Funder id: 10.13039/501100001809, grant no. 61675215) and grant no. 1Z1629051A0001 and Open Research Fund of State Key Laboratory of Pulsed Power Laser Technology, Electronic Engineering Institute.

References

[1] I. J. S, Nature 239, 129–130 (1972).
[2] N. G. Basov, P. Kriukov, S. Zakharov, Yu. Senatsky and S. Tchekalin, IEEE J. Quantum Electron. 4, 864–867 (1968).
[3] D. J. Trummer, R. J. Foley and G. S. Shaw, in 'Proc. SPIE' (1999).
[4] W. H. Williams, J. M. Auerbach, M. A. Henesian, J. K. Lawson, J. T. Hunt, et al., in 'Proc. SPIE.' (1998).
[5] J. Lindl, Phys. Plasmas 2, 3933–4024 (1995).
[6] R. Zacharias, E. Bliss, M. Feldman, A. Grey, M. Henesian, et al., in 'Third International Conference on Solid State Lasers for Application to Inertial Confinement Fusion, Proc. SPIE' (1998).
[7] R. A. Zacharias, N. R. Beer, E. S. Bliss, S. C. Burkhart, S. J. Cohen, et al., Opt. Eng. 43, 2873–2884 (2004).
[8] E. L. Novak, 'Measurement and Analysis Optimization of Large Aperture Laser Fizeau Interferometer', (The University of Arizona, Tucson, 1998).
[9] J. M. Rodenburg and H. M. L. Faulkner, Appl. Phys. Lett. 85, 4795–4797 (2004).
[10] H. M. L. Faulkner and J. M. Rodenburg, Phys. Rev. Lett. 93, 023903-1–023903-4 (2004).
[11] J. R. Fienup, Opt. Lett. 3, 27–29 (1978).
[12] J. R. Fienup, Appl. Opt. 21, 2758–2769 (1982).
[13] J. R. Fienup, Proc. Soc. Photo-Opt. Instrum. Eng. 373, 147–160 (1984).
[14] P. Thibault, M. Dierolf, O. Bunk, A. Menzel and F. Pfeiffer, Ultramicroscopy 109, 338–343 (2009).
[15] R. Hoppe, J. Reinhardt, G. Hofmann, J. Patommel, J -D. Grunwald, et al., Appl. Phys. Lett. 102, 203104-1–203104-4 (2013).
[16] M. K. Yakes, S. B. Qadri, N. A. Mahadik, C. Yi, D. Lubyshev, et al., Appl. Phys. Lett. 101, 241908 (2012).
[17] F. Hue, J. M. Rodenburg, A. M. Maiden and P. A. Midgley, Ultramicroscopy 111, 1117–1123 (2011).
[18] P. Wang, F. Zhang, S. Gao, M. Zhang and A. I. Kirkland, Sci. Rep. 7, 2857 (2017).
[19] H. Wang, S. P. Veetil, C. Liu, J. Wang, W. Huang, et al., Laser Phys. Lett. 12, 025005 (2015).
[20] A. M. Maiden and J. M. Rodenburg, Ultramicroscopy 109, 1256–1262 (2009).
[21] J. W. Goodman, 'Introduction to Fourier Optics. Third edition', (Mc-Graw Hill, New York, 2005).
[22] X. M. Deng, X. Liang, Z. Chen, W. Yu and R. Ma, Appl. Opt. 25, 377–381 (1986).
[23] J. Neauport, X. Ribeyre, J. Daurios, D. Valla, M. Lavergne, et al., Appl. Opt. 42, 2377–2382 (2003).
[24] C. B. W. H. W. Hui and G. Y. G. Lürong, Acta Opt. Sin. 4, 23 (2001).